Journal of Photochemistry & Photobiology, B: Biology 269 (2025) 113208

Contents lists available at ScienceDirect

Journal of Photochemistry & Photobiology, B: Biology

journal homepage: www.elsevier.com/locate/jphotobiol

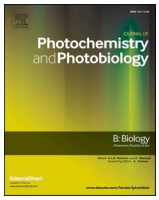

Fluence-dependent infrared photobiomodulation remodels chromatin architecture to enhance chemosensitivity in head and neck tumors

Mariana B. Ramos-Pinto [a,d], Manoela D. Martins [b,c], Cristiane H. Squarize [d], Fabio A. Alves [a,e], Rogerio M. Castilho [d,*]

[a] Department of Stomatology, A.C. Camargo Cancer Center, Sao Paulo, Brazil
[b] Department of Oral Pathology, School of Dentistry, Federal University of Rio Grande do Sul, Porto Alegre, Rio Grande do Sul, Brazil
[c] Department of Oral Diagnosis, Piracicaba Dental School, University of Campinas, Piracicaba, Brazil
[d] Laboratory of Epithelial Biology, Department of Periodontics and Oral Medicine, University of Michigan School of Dentistry, Ann Arbor, MI, United States of America
[e] Department of Stomatology, School of Dentistry, University of São Paulo, São Paulo, Brazil.

ARTICLE INFO

Keywords:
Photobiomodulation
Low-level light therapy
Infrared laser
Chromatin assembly and disassembly
Chemosensitivity
Head and neck neoplasms
Adenoid cystic carcinoma

ABSTRACT

Photobiomodulation (PBM) therapy has emerged as a noninvasive therapeutic modality capable of modulating cellular processes through the targeted delivery of light. In this study, we investigated the effects of an infrared PBM on adenoid cystic carcinoma (ACC) cells, with a focus on fluence-dependent chromatin remodeling and the potential to enhance chemosensitivity to cisplatin. Using a range of energy densities, we observed that up to 26.6 J/cm^2 of PBM induces significant nuclear enlargement and modulates epigenetic markers by increasing histone H4K8 acetylation and decreasing trimethylation of histone H3K9. These changes recapitulate the effects of histone deacetylase inhibitors, previously shown to sensitize tumor cells to chemotherapy. Notably, pre-treatment with a 20 J/cm^2 fluence significantly enhanced cisplatin-induced cell death compared to sham controls, supporting the notion that an open chromatin state can potentiate chemotherapeutic efficacy. In contrast, higher fluences ($\geq$ 33.3 J/cm^2) led to a marked accumulation of DNA double-strand breaks and elevated reactive oxygen species, culminating in increased cell death. Additionally, while PBM consistently reduced cellular proliferation across fluences, it did not affect the migration potential of ACC cells. Owing to its high tissue penetrance, the infrared PBM presents a particularly novel and attractive approach for targeting deep-seated head and neck tumors, including those of salivary gland origin. Collectively, our findings suggest that lower-fluences of infrared PBM represents a safe and effective strategy to remodel tumor chromatin and enhance the chemosensitivity of head and neck cancers, paving the way for its integration into multimodal cancer treatment regimens.

1. Introduction

Throughout history, people have recognized sunlight's critical role in maintaining health, even before modern physiology was understood. Early physicians and natural philosophers observed that exposure to natural light often coincided with improved well-being. Ancient texts from civilizations such as Egypt, Greece, and Persia alluded to the therapeutic benefits of sunlight, noting that controlled exposure could alleviate various ailments. In classical antiquity, figures like Hippocrates and other early medical practitioners acknowledged the sun's influence on the balance of bodily humors, suggesting that sunlight helped restore health by harmonizing internal systems. Across different cultures, sunlight was revered not only for its life-sustaining energy but also for its capacity to prevent and even treat diseases, a concept that later evolved into the practice of heliotherapy, or phototherapy [1]. By the 19th and early 20th centuries, scientists began studying the effects of light on human physiology in greater detail. Niels Ryberg Finsen, the well-known father of ultraviolet therapy from University of Copenhagen, pioneered the use of phototherapy techniques to treat lupus vulgaris and other dermatologic diseases. His contributions into the scientific validation of the healing properties of light were recognized with the Nobel Prize in 1903 [2,3].

* Corresponding author at: Laboratory of Epithelial Biology, Department of Periodontics and Oral Medicine, School of Dentistry, University of Michigan, 1011 N University Ave, Room 3050-Commons, Ann Arbor, MI 48109-1078, United States of America.
E-mail address: rcastilh@umich.edu (R.M. Castilho).

https://doi.org/10.1016/j.jphotobiol.2025.113208
Received 21 April 2025; Received in revised form 25 June 2025; Accepted 27 June 2025
Available online 29 June 2025

Today, phototherapies are widely used in clinical settings through specific physical parameters to safely stimulate healing and enhance overall well-being. Among them, photobiomodulation (PBM) therapy has garnered significant attention as a non-ionizing, noninvasive, and non-thermal approach that utilizes various photon-based sources, including lasers, light-emitting diodes (LEDs), and broadband light, in the visible and near-infrared spectrum. These light sources can modulate cellular metabolism, oxidative stress, and gene expression, contributing to therapeutic outcomes without causing thermal damage [4–6]. PBM uses low-intensity exposure, typically in the range of fractions of milliwatts per square centimeter up to 100 mW/cm^2, ensuring that tissue heating does not exceed 1 °C [7]. If the temperature rises beyond this threshold, the biological effects transition into thermophotobiomodulation, which combines mild hyperthermia with photostimulation, or, in cases involving photosensitizers, may align with photodynamic therapy mechanisms [8,9]. Beyond its local cellular effects, PBM has been shown to confer systemic and long-lasting protective benefits under stress conditions such as oxidative damage, nutrient deprivation, and hypoxia [10]. These include the upregulation of heat shock proteins (e.g., HSP70, HSP90), modulation of pro-inflammatory cytokines, and increased cell viability, even under acute toxic situations [11]. Such outcomes highlight PBM's potential not only for localized therapeutic applications but also for systemic conditioning and possibly long-term effects through mitochondrial or epigenetic pathways. Therefore, careful control of PBM parameters and mechanistic awareness are essential to distinguish its therapeutic effects from other outcomes, and to fully harness its clinical potential.

In regenerative medicine and supportive care in cancer, PBM therapy has proven effective in tissue repair and in preventing severe oral mucositis, as demonstrated in both animal models [12] and clinical trials [13,14]. The photoexcitation of cytochrome *c* oxidase in the mitochondrial electron transport chain remains one of the most widely accepted hypotheses to explain the biological effects of PBM, resulting in increased ATP production, transient generation of reactive oxygen species, and activation of redox-sensitive pathways. These processes facilitate cell proliferation and differentiation but are highly dependent on fluence, exposure duration, and specific cellular conditions [15,16]. However, it is worth to highlight that the exact mechanisms are not fully understood, and additional molecular targets and pathways have also been proposed. Collectively, these PBM therapies are transforming modern clinical practice by offering targeted treatment approaches that significantly improve patient outcomes with no clinical side effects.

In recent years, our laboratory has significantly advanced the understanding of PBM therapy by exploring its safety, efficacy, and underlying molecular mechanisms. Our studies have examined the impact of light therapy on oral carcinogenesis and head and neck squamous cell carcinoma models, revealing important insights into cell proliferation, invasion, and apoptosis [17,18]. Complementary clinical investigations have highlighted its benefits in treating inflammatory conditions such as oral lichen planus, where a PBM source improved healing outcomes while maintaining genomic safety [19,20]. A mechanistic work further demonstrated that PBM therapy triggers reactive oxygen species production and modulates key signaling pathways involved in cellular migration and repair [21,22]. Building upon this robust framework, our most recent research has focused on the PBM-related epigenetic mechanisms. Specifically, using a 660 nm PBM therapy, we observed significant modulation of histone acetylation and methylation patterns, a finding that not only underscores the therapy's ability to regulate gene expression but also contributes to accelerated epithelial healing and stem cell mobilization [23].

Our current study builds on our recent data showing that PBM therapy can modulate chromatin organization in multiple biological contexts, including cancer cells. This compelling evidence has encouraged us to investigate PBM sources able to reach deeper tissue penetration, such as a low-power laser operating in 808 nm infrared wavelength, to modulate the chromatin environment in head and neck cancers. We are focusing on adenoid cystic carcinoma (ACC), a rare salivary gland malignancy distinguished by its unique genetic profile, infiltrative growth, perineural invasion, high metastatic potential, and late recurrences [24]. Given that ACC management still relies on limited therapeutic options—primarily surgical resection, radiotherapy, and systemic therapies that often result in therapy resistance and significant side effects [25,26] —novel strategies are urgently needed. Emerging studies, including our own work with histone deacetylase inhibitors (HDACi) such as Entinostat, Vorinostat, and Scriptaid, have demonstrated that chromatin modulation can sensitize ACC cells to cisplatin by inducing DNA damage and disrupting cancer stem cell populations [27–29]. Therefore, this study aimed to evaluate the biological effects of infrared PBM on ACC, focusing on its ability to stabilize epigenetics and enhance chemo-sensitization to cisplatin.

2. Materials and methods

2.1. Cell line and culture conditions

All the assays utilized the University of Michigan-Human Adenoid Cystic Carcinoma (UM-HACC)-2 A cell line, a GFP-positive cell line derived from a T3N1M0 adenoid cystic carcinoma (ACC) of the minor salivary gland [30]. The cells were cultured in Dulbecco's Modified Eagle's Medium (DMEM) supplemented with 10 % fetal bovine serum (FBS) (HyClone, Logan, UT, USA), 2 mM L-glutamine (Gibco, Waltham, MA, USA), 20 ng/mL human epidermal growth factor (Sigma-Aldrich, St. Louis, MO, USA), 400 ng/mL hydrocortisone (Sigma-Aldrich), 5 μg/mL insulin (Sigma-Aldrich), and a cocktail of antibiotic/antimycotic solution containing 10,000 units of penicillin, 10,000 μg of streptomycin, and 25 μg of amphotericin B per mL (HyClone, Logan, UT, USA). The cells were incubated in a 5 % CO_2-humidified incubator at 37 °C. The UM-HACC-2 A GFP-positive cells were seeded on culture plates and cultivated until reaching approximately 70 % cellular confluency for the assays. Cell stress was induced by reducing the FBS concentration to 3 % (regular cell media with 3 % FBS, nutritional deficit).

2.2. Photobiomodulation therapy

The PBM protocols were performed using a continuous Indium-Gallium-Aluminum-phosphide (InGaAlP) diode laser (Laser DUO, MM Optics Ltd., São Carlos, Brazil) in a punctual application mode. The laser parameters were previously calibrated using a power meter (Laser Check; MM Optics Ltd., São Carlos, Brazil) by a single trained professional wearing protective eyewear. All the protocols included an infrared wavelength of 808 nm, with a fiber with spot area of 0.03 cm^2 (approximately 1.95 mm in diameter) as specified by the manufacturer, a fixed average power of 100 mW confirmed using a calibrated power meter, irradiance of 3.33 W/cm^2, but distinct energy densities or fluences (J/cm^2) due to different exposure times. In addition to conventional fluence (J/cm^2), we also reported photon fluence (p.J/cm^2 and Einstein units) to reflect the wavelength-dependent energy of photons. Both units are presented to support reproducibility and facilitate clinical translation (Table 1).

All the laser irradiations were performed by directing the laser from below through the transparent glass bottom of black-walled 96-well plates (Cellvis, P96–1.5H-N), which feature #1.5 cover glass (0.170 ± 0.005 mm thickness) and an internal well diameter of approximately 6.2 mm. The laser handpiece, with a distal tip diameter of approximately 6.0 to 6.2 mm, was positioned at a 90° angle relative to the plate and placed in direct contact with the outer glass surface. This close matching between the tip and well diameter ensured centralized alignment and reduced lateral beam escape. The beam was centered at the bottom of each well. All experiments were conducted under partially dark conditions to avoid ambient light interference. Additionally, to prevent cross-irradiation between wells, plates with black polystyrene walls were used. Control groups underwent identical handling procedures,

Table 1
Physical parameters of photobiomodulation protocols.*

Common parameters	PBM source	Protocols	Fluence (J/cm^2)	Energy per point (J)	Time (seconds)	Photon fluence (p. J/cm^2)	Photon fluence (Einstein)
Type	Indium-Gallium-Aluminum Phosphide Diode Laser	Control	0	0	0	0	0
Wavelength (nm)	808	1st	3.33	0.1	1	5	1
Operational mode	Continuous	2nd	6.67	0.2	2	10	2
Frequency (Hz)	~ 50/60	3rd	13.3	0.4	4	20	4
Pulse duration (ms)	Continuous	4th	20.0	0.6	6	30	7
Peak power (W)	0.01	5th	26.6	0.8	8	40	9
Average power (mW)	100	6th	33.3	1	10	51	11
Polarization	Yes	7th	40.0	1.2	12	61	14
Spot area (cm^2)	0.03	8th	46.6	1.4	14	71	16
Beam shape	Circular	9th	53.3	1.6	16	82	18
Beam profile	Gaussian	10th	60.0	1.8	18	92	20
Irradiance (W/cm^2)	3.33	11th	66.6	2	20	102	23

* The photon energy used was 1.54 eV (rounded) according to the wavelength (808 nm).

including laser positioning, but with the PBM device turned off (sham irradiation).

2.3. Morphological and volumetric nuclear analysis

To assess changes in the nuclei over time after PBM exposure, a total of 4 × 10^3 UM-HACC-2 A GFP-positive cells were seeded on 96-well glass-bottom black plates (Cellvis Cat# P96–1.5H-N) in four replicates per group and maintained at 37 °C for 24 h to allow normal growth. Subsequently, the cells received a single laser session (808 nm, 100 mW, 3.33 W/cm^2, 0.03 cm^2, 20 J/cm^2, 30.7 p.J/cm^2, 6 s.) at each respective time point (groups: control, 30 s., 1 min., 2 min., 5 min., 10 min., 20 min., 30 min., 40 min., 50 min., and 60 min.). After irradiation, the cells were fixed with 4 % paraformaldehyde for 20 min, followed by three washes with 1× phosphate-buffered saline (PBS) every three minutes. All the cells were then stained with Hoechst 33342 (1:500, Invitrogen) to visualize the DNA content. Images of 9 fields (confocal, 20× magnification) of each well were captured and quantified using the Molecular Devices Image Xpress Micro 4 system through the DAPI filter. Then, five outcomes were used to assess nuclear alterations: total area (μm^2), perimeter (μm), granularity area (% of heterochromatin), texture index (chromatin heterogeneity) and shape factor (circularity) (Fig. 1A).

2.4. Immunofluorescence analyses

To evaluate alterations in chromatin dynamics, proliferation index, and DNA damage, a total of 2.5 × 10^3 UM-HACC-2 A GFP-positive cells were seeded on 96-well glass-bottom black plates (Cellvis Cat# P96–1.5H-N) in eight replicates per group and maintained for 24 h at 37 °C until normal growth. Once the cells were well adhered, the culture media was replaced with nutritional-deficit media (3 % FBS) in all groups for 48 h. After the stress condition, twelve groups were established: a control group (no laser) and eleven laser groups (3.33 J/cm^2 to 66.6 J/cm^2). The PBM groups received three laser sessions, every 6 h (0, 6, 12 h), respecting the specific laser protocols described in Table 1. After the last laser session, all the cells were fixed with 4 % paraformaldehyde for 20 min, followed by three washes with 1× phosphate-buffered saline (PBS) every three minutes. Subsequently, the cells were blocked with 1 % PBS/BSA + 0.5 % Triton X-100 for 60 min and then incubated overnight with the following primary antibodies: anti-trimethyl-histone H3 Lys 9 (1:400; Cell Signaling Technology, Danvers, MA, USA), anti-acetyl Histone H4 Lys 8 (1:100; Thermo Fisher Scientific Inc.), phospho-Histone H2A.X (Ser 139) (1:100; Cell Signaling Technology), and Ki67 (1:5; Developmental Studies Hybridoma Bank, IA, USA). After three washes in 1× PBS, the cells were incubated with Alexa 568 and 633 as secondary antibodies and stained with Hoechst 33342 (1:500, Invitrogen) for DNA content (DAPI) visualization. Images of 9 fields (widefield, 20× magnification) of each well were captured and quantified using the Molecular Devices ImageXpress Micro 4 system through the Texas Red, Cy5, and DAPI filters. Non-irradiated cells receiving only secondary antibodies were considered as negative controls.

2.5. Oxidative stress and cell viability assay

To investigate the variations in oxidative stress and cell death in live ACC cells, a total of 5 × 10^3 UM-HACC-2 A GFP-positive cells were seeded on 96-well glass-bottom black plates (Cellvis Cat# P96–1.5H-N) in eight replicates per group and maintained for 24 h at 37 °C until normal growth. Then, the culture media was replaced with nutritional-deficit media (3 % FBS) in all groups for 48 h. At 48 h of the starvation condition, the PBM groups received three laser sessions, every 6 h (0, 6, 12 h), following the protocols described in Table 1. After the last laser session, levels of reactive oxygen species (ROS) were detected using a ROS-sensitive fluorescent dye (1:500, CellROX™ Deep Red Reagent, Invitrogen), cell death was assessed through propidium iodide (PI) staining (1:1000, Biotium #40048), and DNA content was evaluated with Hoechst 33342 (1:500, Invitrogen). The cells were simultaneously incubated with these reagents at 37 °C for 30 min. Images of 4 fields (widefield, 4× magnification) and 9 fields (widefield, 20× magnification) of each well were captured and quantified using the Molecular Devices ImageXpress Micro 4 system through the Cy5 filter (ROS), Texas Red (PI), and DAPI (Hoechst) channels. Positive controls were treated with 400 mM hydrogen peroxide for 30 min.

2.6. Scratch assay

To explore the migration potential, a total of 1.5 × 10^5 UM-HACC-2 A GFP-positive cells were seeded on 12-well culture plates in triplicate for each group: vehicle (no laser), 20 J/cm^2, 40 J/cm^2 and 60 J/cm^2. After 6 h (when the cells were attached), the culture media was replaced with nutritional-deficit media (3 % FBS) in all groups for 16 h. After 24 h from cell seeding (time zero – T0), two perpendicular crossing scratches (lines) were performed in each well containing cells at 100 % confluency utilizing a 200 μL pipette tip. After three washes with PBS, PBM groups were exposed to three sessions of four punctual irradiations with 6 h of interval as proposed by Martins et al. 2020 [31], and the wound closure was evaluated at 0, 6, 12, 24, and 30 h. Images of the wound areas were collected at each time point using an inverted microscope (EVOS Cell Imaging Systems, Seoul, Republic of Korea). The percentage of the relative wound closure was based on four regions of interest measured using image analysis software (ImageJ 1.52v, Bethesda, MD, USA).

2.7. Statistical analysis

All statistical analyses were performed using GraphPad Prism 10.0 software (GraphPad Software, San Diego, CA, USA). One-way analysis of variance (ANOVA) followed by Tukey's multiple comparison test was used for all statistical comparisons. Asterisks denote statistical significance, with *p*-values reported as follows: $*p < 0.05$, $**p < 0.01$, $***p < 0.001$, $****p < 0.0001$.

3. Results

3.1. Lower-fluence infrared PBM modifies nuclear size, morphology and chromatin organization

Nuclear morphology analysis revealed that a single session of PBM therapy at 20 J/cm^2 induced a rapid and sustained statistically significant expansion in nuclear area. The nuclear enlargement began as early as 30 s post-irradiation ($p = 0.017$), peaked at 1 min ($p < 0.0001$), and remained significantly enlarged up to 60 min ($p = 0.002$) (Fig. 1A). Initially, nuclei exhibited a homogeneous enlargement during early post-PBM time points (30 s. – 5 min). However, at later periods, some nuclei displayed irregular contours and reduced compactness, suggesting nuclear remodeling potentially associated with chromatin decondensation and alterations in cytoskeletal-nuclear interactions.

Supporting this, perimeter measurements revealed a significant increase from baseline, reflecting more complex or irregular nuclear outlines. Furthermore, PBM led to a transient elevation in the nuclear texture index, particularly evident between 30- and 40-min post-irradiation, indicating increased chromatin heterogeneity likely due to euchromatin expansion. This interpretation is reinforced by a significant reduction in granular area (heterochromatin content) mainly within the first 10 min post-PBM. Lastly, a gradual decrease in the nuclear shape factor was observed, indicating a time-dependent shift from regular circular nuclei towards more irregular or kidney-shaped morphologies, consistent with a dynamic structural reorganization of the nucleus likely due to chromatin organization (Fig. 1A).

We next investigated the effects of different fluences on chromatin organization by examining two key epigenetic markers. PBM modulated chromatin architecture by promoting chromatin acetylation through reduced chromatin methylation while maintaining euchromatin integrity at lower fluences (3.33–26.6 J/cm^2). Specifically, histone H4K8 acetylation (H4K8ac) levels and trimethylation of histone H3K9 (H3K9me3) were analyzed (Fig. 1B and C). Specifically, histone H4K8 acetylation (H4K8ac), a marker of transcriptionally active euchromatin associated with chromatin relaxation and gene expression, and trimethylation of histone H3K9 (H3K9me3), a marker of condensed heterochromatin typically linked to gene silencing and chromatin compaction, were analyzed (Fig. 1B and C).

At higher fluences ($\geq$ 33.3 J/cm^2), a substantial increase in H3K9me3 levels was observed, with a peak at 40 J/cm^2, indicating compensatory heterochromatin formation. Concurrently, a progressive decline in H4K8ac-positive cells was detected from 33.3 J/cm^2, becoming statistically significant ($p = 0.0003$). This reduction in histone acetylation suggests a potential decrease in transcriptional activity and promotion of chromatin compaction. These findings demonstrate that PBM may differentially regulate epigenetic states depending on the applied fluence, with potential implications for transcriptional regulation and cellular responses.

3.2. Exposure to higher-fluence PBM leads to the accumulation of DNA damage and subsequent cell death

To explore these cytotoxic effects, we measured three interconnected parameters: γ-H2AX levels (a marker of DNA double-strand breaks), propidium iodide (PI) staining (an indicator of cell death), and intranuclear reactive oxygen species (ROS) levels. γ-H2AX levels increased gradually from 3.33 to 33.3 J/cm^2 and then spiked sharply between 40 and 46.6 J/cm^2 ($p < 0.0001$), eventually stabilizing at roughly 50 % DNA damage at the highest fluences. Although PI staining initially indicated only modest cell death, higher PBM fluences generated a delayed yet statistically significant increase in cell death compared to the control, with a peak observed at 33.3 J/cm^2 ($p < 0.0001$). In parallel, the quantification of ROS-positive nuclei revealed a fluence-dependent escalation in oxidative stress, showing minimal changes at doses up to 20 J/cm^2, followed by a dramatic rise at 60–66.6 J/cm^2 ($p < 0.0001$). These findings indicate that PBM at fluences of 33.3 J/cm^2 and above results in a significant accumulation of DNA double-strand breaks that ultimately leads to cell death—a process that does not appear to be driven by cumulative intracellular oxidative stress, as ROS levels only reach a critical threshold at the highest fluences (Fig. 2A, B, and C).

3.3. Infrared PBM decreases cellular proliferation without affecting migration across all fluences

Infrared PBM (808 nm) was applied to ACC cells at various energy densities to evaluate its effects on both cellular proliferation and migration. Ki67 expression served as a marker for proliferation, and all tested PBM protocols led to a significant reduction in Ki67-positive cells compared to controls, with the greatest decrease observed at fluences between 26.6 and 40 J/cm^2 ($p < 0.0001$). This pronounced decrease indicates that the infrared PBM not only suppresses mitotic activity but may also reallocate cellular energy towards damage repair and differentiation, reflecting a potential biphasic response. In parallel experiments assessing cell migration, we observed no significant changes in the migration potential of cells over a 30-h period across all fluences (Fig. 3B). These data suggest that while infrared PBM consistently diminishes cellular proliferation, it does not compromise the cells' migratory capabilities regardless of the energy dose applied.

3.4. Potential of low fluence infrared PBM to enhance chemosensitivity in ACC tumor cells

Building on our previous findings that HDACi sensitize tumor cells to therapy by acetylating chromatin—thereby increasing transcriptional activity through conversion to euchromatin—we evaluated whether low fluence infrared PBM could achieve similar chromatin remodeling in ACC tumor cells. Our results demonstrate that infrared PBM induces the acetylation of histone H4K8 while reducing levels of trimethylated histone H3K9 at fluences up to 26.6 J/cm^2 (Fig. 1B and C). Notably, when cells were exposed to an infrared PBM at 20 J/cm^2 of fluence prior to treatment with the chemotherapeutic agent cisplatin (CDDP), a significant increase in cell death was observed compared to sham controls (Fig. 4A and B). These data indicate that low fluence infrared PBM effectively 'opens' the cancer cell chromatin, thereby enhancing sensitivity to chemotherapy and suggesting a novel therapeutic strategy to manage cancers without relying on the additional toxic effects associated with chemical sensitizers (Fig. 4C).

4. Discussion

The use of light for therapeutic purposes has ancient origins. For centuries, civilizations recognized its potential to promote health and healing - a concept that evolved into modern phototherapy [32]. Nowadays, PBM therapy is considered a cutting-edge tool that takes advantage of specific visible and infrared wavelengths, to modulate a wide range of biological events. Transitioning from bench to the bedside scenario, PBM therapy has been described as a non-invasive and patient-friendly treatment modality successfully applied from accelerating wound healing to enhancing tissue regeneration [13,14]. Building upon this robust background and our previous findings on PBM modulating chromatin architecture, our current study explored how PBM influences tumor cell behavior ultimately contributing to chemosensitization.

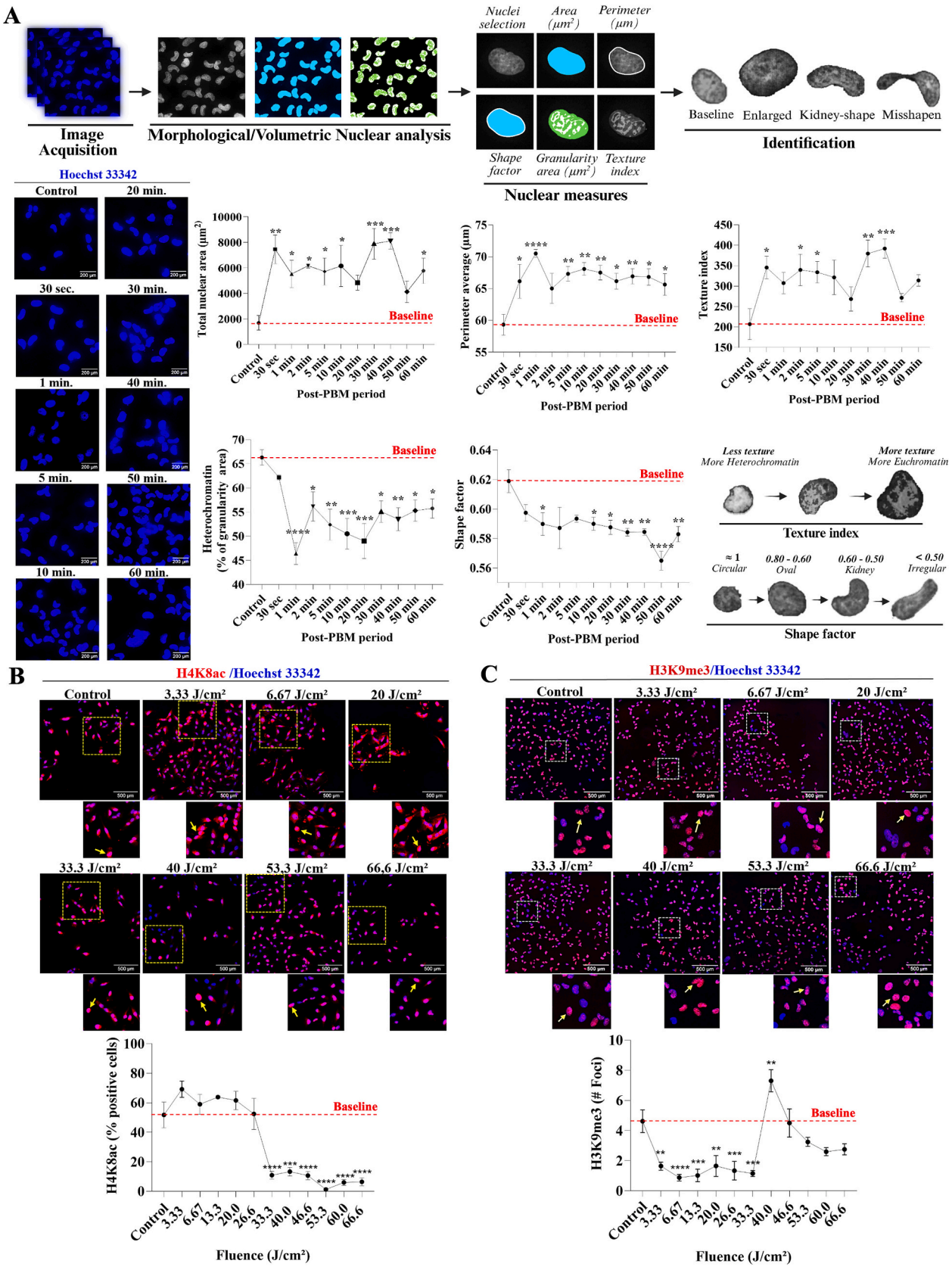

Fig. 1. Photobiomodulation (PBM) induces chromatin structural changes. (A) Morphological and volumetric nuclear analysis demonstrating chromatin decompaction following a single low-fluence of a diode laser irradiation session. (B) High-fluence PBM results in decreased H4K8ac expression, indicative of reduced euchromatin. (C) Low-fluence PBM causes minimal H3K9me3 foci levels, suggesting limited heterochromatin modification. Statistical significance is indicated as $*p < 0.05$, $**p < 0.01$, $***p < 0.001$, $****p < 0.0001$.

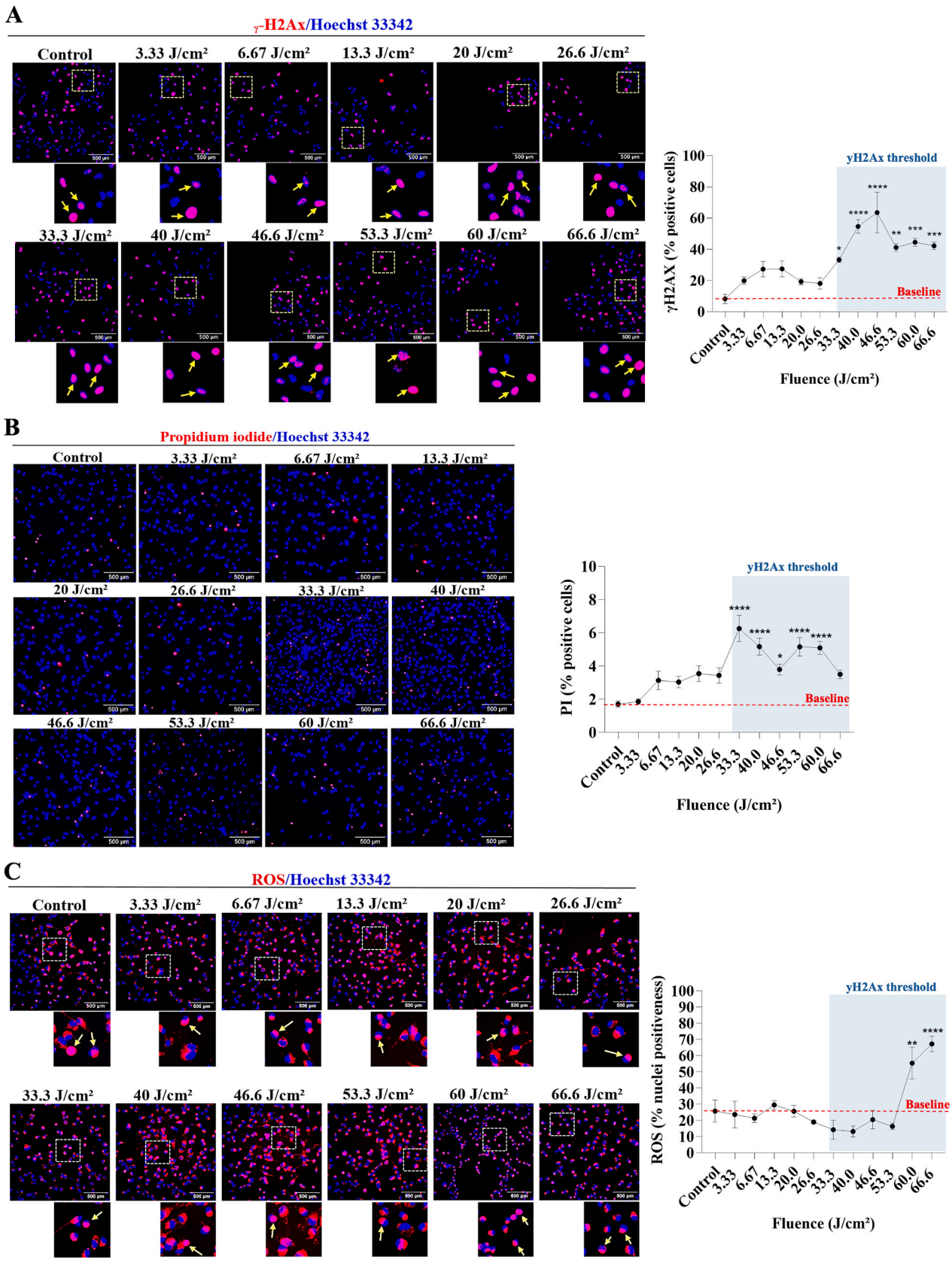

Fig. 2. Effects of high-fluence photobiomodulation (PBM) on cellular damage and stress. (A) High-fluence PBM stimulates the accumulation of DNA double-strand breaks. (B) High-fluence PBM induces a modest increase in cell death. (C) Significant nuclear reactive oxygen species (ROS) levels are observed only at the highest fluences (over 60 J/cm^2). Statistical significance is indicated as *p < 0.05, **p < 0.01, ***p < 0.001, ****p < 0.0001.

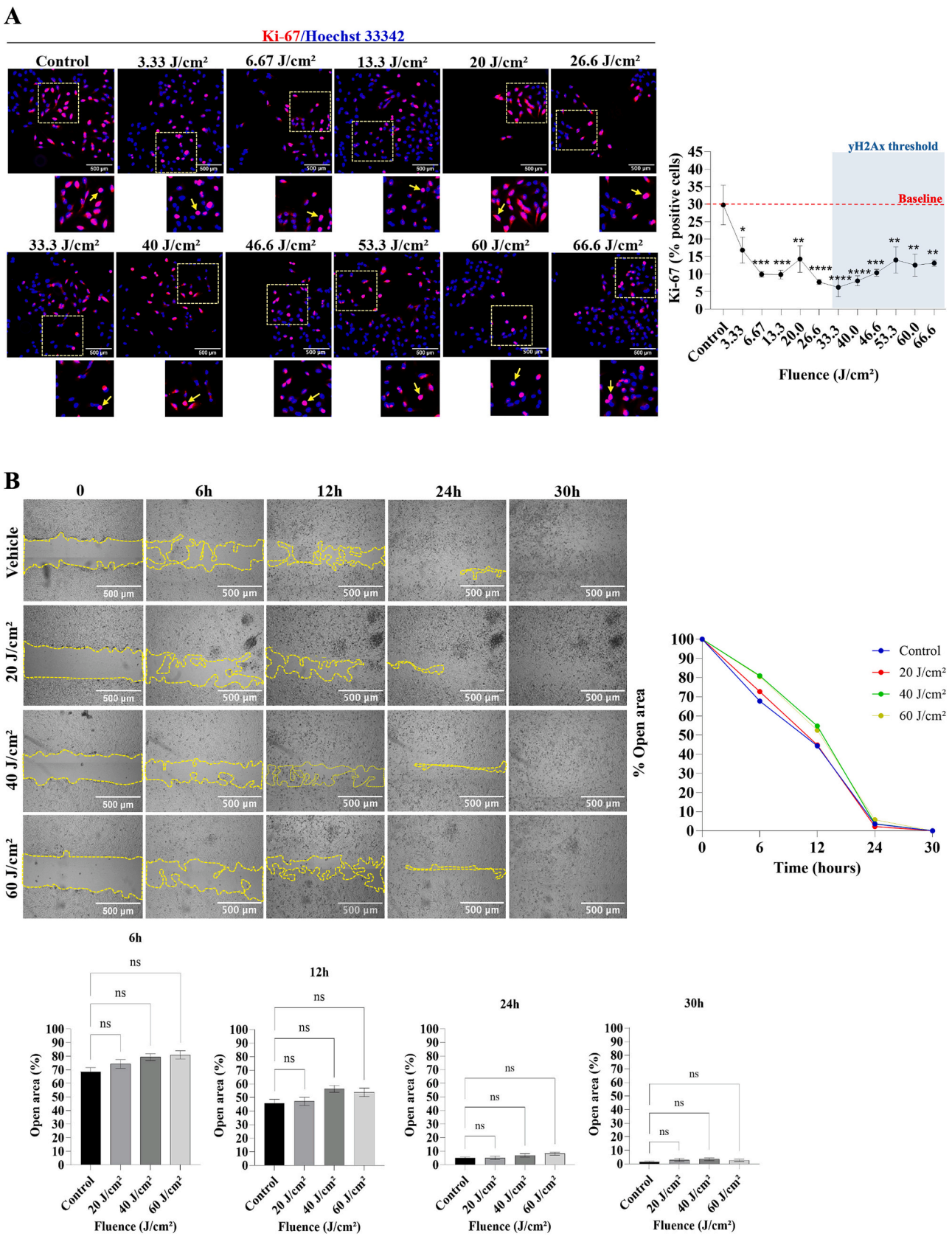

Fig. 3. Impact of infrared diode laser therapy on cellular behavior. (A) Infrared diode laser therapy leads to a reduction in cell proliferation across different fluence levels. (B) Cellular migration potential shows no significant changes over a 30-h period between vehicle control and fluences of 20, 40, and 60 J/cm^2. Statistical significance is indicated as *p < 0.05, **p < 0.01, ***p < 0.001, ****p < 0.0001.

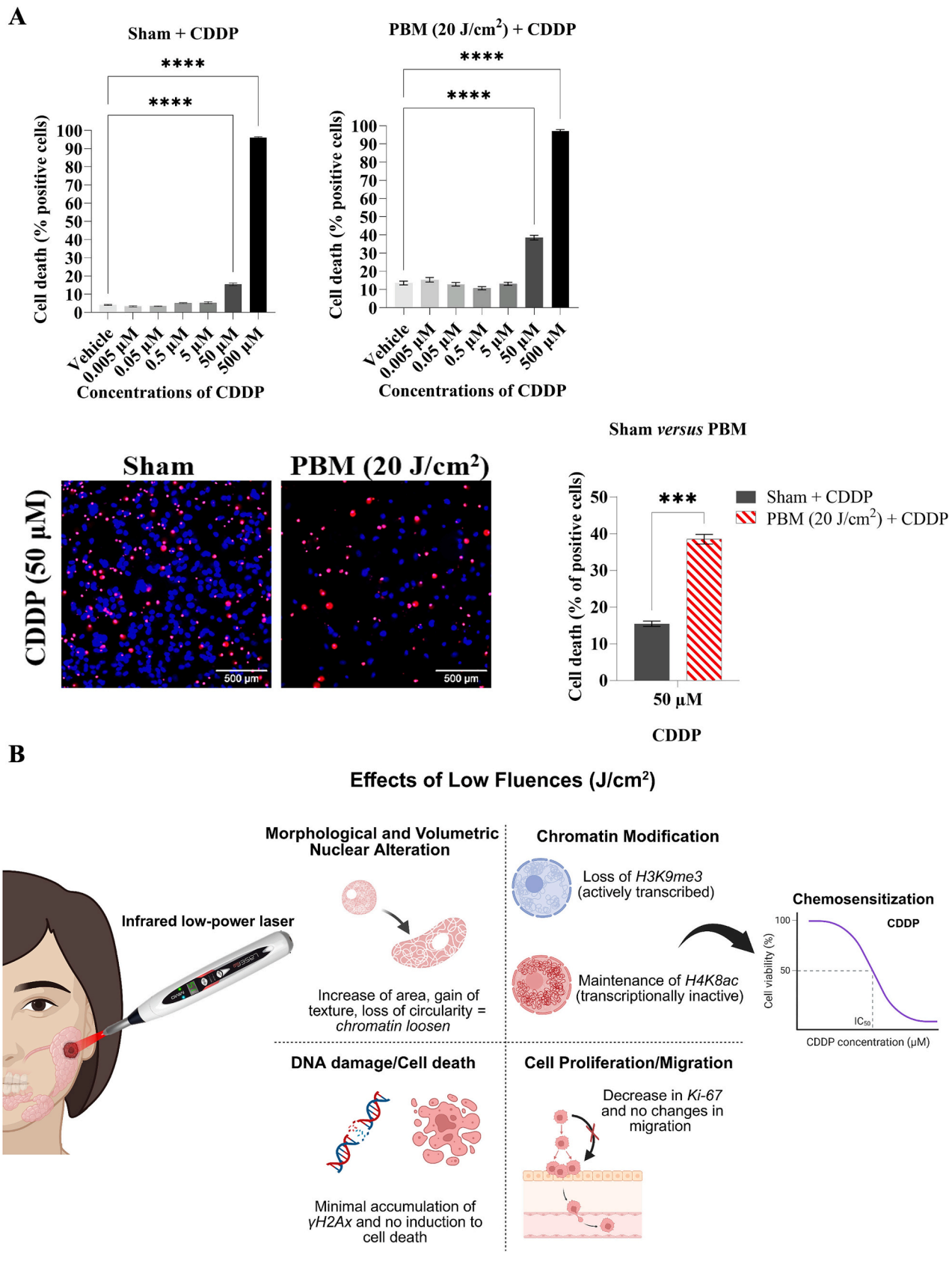

Fig. 4. Photobiomodulation (PBM) effects on cisplatin-induced cell death in adenoid cystic carcinoma (ACC). (A) Infrared diode laser therapy at 20 J/cm^2 fluence, administered prior to cisplatin (CDDP) treatment, significantly increases cell death compared to sham controls. (B) Schematic illustration summarizing the effects of low-fluence PBM in adenoid cystic carcinoma. Statistical significance is indicated as *p < 0.05, **p < 0.01, ***p < 0.001, ****p < 0.0001.

Our data revealed that the application of an infrared PBM therapy through a diode laser modulates tumor chromatin in a fluence-dependent manner. At lower fluences (up to 26.6 J/cm^2), we primarily observed an increase of nuclear area, gain of nuclear texture and loss of nuclear circularity denoting a chromatin architecture reorganization towards loosening. On a deeper level, we noticed a maintenance of the acetylation of H4K8 levels compared to the baseline, a marker of transcriptionally active euchromatin, along with a concomitant decrease in the levels of the trimethylated form of histone H3K9, a marker of condensed heterochromatin (Fig. 1B and C). These alterations in the epigenetic landscape resemble the effects seen with HDACi, which have been previously shown in our laboratory to sensitize tumor cells to chemotherapy by opening the chromatin structure, promoting gene expression and redirecting cellular energy away from proliferation [33].

In our investigation with ACC cell culture—a representative model for challenging head and neck tumors—we further demonstrated that the beneficial chromatin remodeling induced by a low fluence PBM protocol can be harnessed to enhance the efficacy of chemotherapy. Specifically, pre-treatment of ACC cells with three sessions of PBM therapy (808 nm, 100 mW, 3.33 W/cm^2, 20 J/cm^2, 0.6 J, 6 s.) resulted in a significant increase in cell death following exposure to cisplatin (CDDP) compared to sham-treated controls (Fig. 4A and B). Similarly to our findings, Barasch et al. 2015 [34] reported that a pre-exposure to a helium-neon (He-Ne) at a visible wavelength (632.8 nm) combined with ionizing radiation (IR) enhanced the tumor cell death of leukemia cells, whereas protecting normal lymphoblasts from IR at the same low fluence of 4 J/cm^2. Briefly, these data strengthen the growing consensus that low-fluence of PBM therapy holds promise as an adjuvant sensitizing tool in both chemotherapy and radiotherapy, improving therapeutic outcomes without relying on additional chemical sensitizers, thereby improving overall treatment outcomes (Fig. 4C).

Moreover, the parameters-dependent effects of PBM therapy are particularly noteworthy. While lower-fluence protocols promoted beneficial chromatin modifications and chemosensitization, our results also indicated a paradox where higher fluences ($\geq$33.3 J/cm^2) provoked adverse effects, including the accumulation of DNA double-strand breaks, an increase of nuclear ROS at the highest fluences, and subsequent cell death. This biphasic response highlights the importance of finely calibrating the PBM physical parameters, to ensure that the therapeutic window is optimized to improve chemosensitivity without inducing cytotoxicity through excessive DNA damage [35]. Another key aspect of our findings is the use of an 808 nm infrared laser, selected for its superior tissue penetration capacity [36]. This feature is particularly advantageous for head and neck malignancies—especially those originating in the salivary glands—which are often embedded in deep or anatomically complex regions. The enhanced penetrative ability of infrared PBM therapy enables effective delivery of PBM effects, such as chromatin remodeling and chemosensitization, even in tumors that are otherwise difficult to reach. This characteristic expands the potential applicability of PBM to a broader range of solid tumors in the head and neck area and may offer a transformative approach to improving therapeutic access and outcomes in these challenging cancers.

In addition to enhancing chemosensitivity, our data indicate that infrared PBM therapy decreased cellular proliferation across all fluences without affecting migration. The reduction in Ki67 expression observed in PBM-treated cells suggests an inhibition of mitotic activity and a possible realignment of cellular metabolism towards DNA repair and differentiation. Notably, the fact that migration remained unchanged is a favorable outcome, as it suggests that while tumor growth is restrained, there is no unintended stimulation of invasive behavior. This aligns with existing literature, which highlights that PBM elicits distinct biological responses depending on cell type and PBM settings [37]. In cancer models, PBM therapy has been shown not to promote tumor progression or invasiveness; rather, it can inhibit proliferation and enhance sensitivity to antineoplastic therapies in a safe and clinically relevant manner [38–40].

Taken together, our study provides compelling evidence that low-fluence infrared PBM therapy can remodel tumor chromatin to create a more transcriptionally active state, thereby sensitizing head and neck tumor cells to chemotherapy. The deep tissue penetrance of the 808 nm infrared laser further enhances its clinical applicability, making it a promising adjunctive treatment option for ACC and other challenging head and neck cancers. As our understanding of the underlying epigenetic mechanisms continues to evolve, future studies should focus on refining laser parameters and integrating PBM into multimodal treatment strategies, with the goal of achieving improved patient outcomes while minimizing the systemic toxicities associated with conventional chemotherapy.

5. Conclusion

This study demonstrates that infrared low-power laser exerts fluence-dependent effects on nuclear architecture, chromatin organization, and cellular behavior in adenoid cystic carcinoma (ACC) cells. Low fluences ($\leq$26.6 J/cm^2) induced dynamic nuclear remodeling and euchromatin enrichment via H4K8 acetylation while maintaining nuclear integrity and minimal DNA damage, supporting its role in promoting a transcriptionally active state. In contrast, higher fluences ($\geq$33.3 J/cm^2) led to chromatin compaction, DNA double-strand breaks, and reduced cell viability, highlighting a cytotoxic threshold. Importantly, PBM at 20 J/cm^2 not only suppressed proliferation but also enhanced chemosensitivity to cisplatin without impairing cell migration, suggesting a promising adjuvant role for PBM in cancer therapy through chromatin priming. Together, these findings position low fluence infrared PBM as a potent, noninvasive epigenetic modulator capable of enhancing therapeutic response while preserving cell motility, opening new avenues for precision PBM-based combinatorial strategies in oncology.

CRediT authorship contribution statement

Mariana B. Ramos-Pinto: Writing – review & editing, Writing – original draft, Visualization, Validation, Software, Methodology, Investigation, Formal analysis, Data curation, Conceptualization. **Manoela D. Martins:** Writing – review & editing, Writing – original draft, Visualization, Validation, Software, Methodology, Investigation, Formal analysis, Data curation, Conceptualization. **Cristiane H. Squarize:** Writing – review & editing, Writing – original draft, Visualization, Validation, Software, Resources, Project administration, Methodology, Investigation, Funding acquisition, Formal analysis, Data curation, Conceptualization. **Fabio A. Alves:** Writing – review & editing, Writing – original draft, Visualization, Validation, Methodology, Formal analysis, Data curation, Conceptualization. **Rogerio M. Castilho:** Writing – review & editing, Writing – original draft, Visualization, Validation, Supervision, Software, Resources, Project administration, Methodology, Investigation, Funding acquisition, Formal analysis, Data curation, Conceptualization.

Declaration of generative AI and AI-assisted technologies in the writing process

During the preparation of this work, the authors used UM-GPT to enhance the readability and language of the manuscript. After using this tool, the authors reviewed and edited the content as necessary and take full responsibility for the content of the published article. The final schematic representation was created using BioRender.

Declaration of competing interest

The authors declare that they have no known competing financial interests or personal relationships that could have appeared to influence the work reported in this paper.

Acknowledgments

This work was supported by the University of Michigan Faculty Research funds. The authors would like to thank the Brazilian Federal Agency for Support and Evaluation of Graduate Education (CAPES) for the Dr. Ramos-Pinto scholarship, and the Brazilian National Institute of Science and Technology in Translational Biophotonics in Dentistry (408830/2024-7) from the Brazilian National Council for Scientific and Technological Development (CNPq).

Data availability

Data will be made available on request.

References

[1] A. Grzybowski, J. Sak, J. Pawlikowski, A brief report on the history of phototherapy, Clin. Dermatol. [Internet]. 34 (2016) 532–537. Available from, https://linkinghub.elsevier.com/retrieve/pii/S0738081X16301341.
[2] H. Hönigsmann, History of phototherapy in dermatology, Photochem. Photobiol. Sci. [Internet]. 12 (2012) 16–21. Available from: https://doi.org/10.1039/c2pp25120e.
[3] A. Grzybowski, K. Pietrzak, From patient to discoverer—Niels Ryberg Finsen (1860–1904)—the founder of phototherapy in dermatology, Clin. Dermatol. [Internet]. 30 (2012) 451–455. Available from, https://linkinghub.elsevier.com/retrieve/pii/S0738081X11003543.
[4] J.J. Anders, P.R. Arany, G.D. Baxter, R.J. Lanzafame, Light-emitting diode therapy and low-level light therapy are Photobiomodulation therapy, Photobiomodul. Photomed. Laser Surg. 37 (2019) 63–65.
[5] L.F. de Freitas, M.R. Hamblin, Proposed mechanisms of Photobiomodulation or low-level light therapy, IEEE J. Sel. Top. Quantum Electron. 22 (2016) 348–364.
[6] M.R. Hamblin, Mechanisms and mitochondrial redox signaling in Photobiomodulation, Photochem. Photobiol. 94 (2018) 199–212.
[7] R. Zein, W. Selting, M.R. Hamblin, Review of light parameters and photobiomodulation efficacy: dive into complexity, J. Biomed. Opt. 23 (2018) 1.
[8] R.K. Chailakhyan, A.G. Grosheva, N.N. Vorob'eva, A.P. Sviridov, V.I. Yusupov, Laser Thermo-Photobiomodulation of bone marrow mesenchymal stem cells, Bull. Exp. Biol. Med. 174 (2023) 523–526.
[9] Y.S. Romanko, A.F. Tsyb, M.A. Kaplan, V.V. Popuchiev, Relationship between antitumor efficiency of photodynamic therapy with Photoditasine and Photoenergy density, Bull. Exp. Biol. Med. 139 (4) (2005) 460–464.
[10] P. Bikmulina, N. Kosheleva, A. Shpichka, V. Yusupov, V. Gogvadze, Y. Rochev, et al., Photobiomodulation in 3D tissue engineering, J. Biomed. Opt. 27 (2022).
[11] E.G. Novoselova, O.V. Glushkova, M.O. Khrenov, D.A. Cherenkov, S.M. Lunin, T. V. Novoselova, et al., Protective effect of low-intensity laser irradiation under acute toxic stress, Biophysics (Oxf). 52 (2007) 83–86.
[12] B.C. Mármora, F.T. Brochado, T.R. Schmidt, L.G. Santos, A.A. de Araújo, C.A.C. X. de Medeiros, et al., Defocused high-power diode laser accelerates skin repair in a murine model through REDOX state modulation and reepithelization and collagen deposition stimulation, J. Photochem. Photobiol. B 225 (2021) 112332.
[13] Y. Zadik, P.R. Arany, E.R. Fregnani, P. Bossi, H.S. Antunes, R.-J. Bensadoun, et al., Systematic review of photobiomodulation for the management of oral mucositis in cancer patients and clinical practice guidelines, Support Care Cancer 27 (2019) 3969–3983.
[14] J. Robijns, R.G. Nair, J. Lodewijckx, P. Arany, A. Barasch, J.M. Bjordal, et al., Photobiomodulation therapy in management of cancer therapy-induced side effects: WALT position paper 2022, Front. Oncol. Front. Media S.A. 12 (2022) 927685.
[15] T. Karu, L. Pyatibrat, G. Kalendo, Irradiation with HeNe laser increases ATP level in cells cultivated in vitro, J. Photochem. Photobiol. B 27 (1995) 219–223.
[16] T.I. Karu, L.V. Pyatibrat, N.I. Afanasyeva, A novel mitochondrial signaling pathway activated by visible-to-near infrared radiation, Photochem. Photobiol. 80 (2004) 366–372.
[17] M.D. Martins, F.M. Silveira, L.P. Webber, V.P. Wagner, M.A.T. Martins, C. H. Squarize, et al., The impact of photobiomodulation therapy on the biology and behavior of head and neck squamous cell carcinomas cell lines, J. Photochem. Photobiol. B 209 (2020) 111924.
[18] L.F. Schuch, D. Campagnol, T.R. Schmidt, C.H.T. Michel, T.N.A. Garcez, V. R. Velho, et al., Investigating the safety of photobiomodulation in oral carcinogenesis: insights into cell proliferation, invasion, and apoptosis via the 4NQO model, Sci. Rep. 14 (2024) 28303.
[19] C.S. Dillenburg, M.A.T. Martins, M.C. Munerato, M.M. Marques, V.C. Carrard, M. Sant'Ana Filho, et al., Efficacy of laser phototherapy in comparison to topical clobetasol for the treatment of oral lichen planus: a randomized controlled trial, J. Biomed. Opt. 19 (2014) 068002.
[20] C.S. Dillenburg, M.A.T. Martins, L.O. Almeida, L. Meurer, C.H. Squarize, M. D. Martins, et al., Epigenetic modifications and accumulation of DNA double-Strand breaks in Oral lichen planus lesions presenting poor response to therapy, Medicine 94 (2015) e997.
[21] C.S. Dillenburg, L.O. Almeida, M.D. Martins, C.H. Squarize, R.M. Castilho, Laser phototherapy triggers the production of reactive oxygen species in oral epithelial cells without inducing DNA damage, J. Biomed. Opt. 19 (2014) 048002.
[22] A.C.A. Pellicioli, M.D. Martins, C.S. Dillenburg, M.M. Marques, C.H. Squarize, R. M. Castilho, Laser phototherapy accelerates oral keratinocyte migration through the modulation of the mammalian target of rapamycin signaling pathway, J. Biomed. Opt. 19 (2014) 028002.
[23] M.D. Martins, F.M. Silveira, M.A.T. Martins, L.O. Almeida, V.S. Bagnato, C. H. Squarize, et al., Photobiomodulation therapy drives massive epigenetic histone modifications, stem cells mobilization and accelerated epithelial healing, J. Biophotonics 14 (2021) e202000274.
[24] E. Saleh, A. Ukwas, Adenoid cystic carcinoma of salivary glands: a ten-year review and an assessment of the current management, surgery, radiotherapy, and chemotherapy, Int. J. Otolaryngol. 2023 (2023) 1–16.
[25] J.L. Geiger, N. Ismaila, B. Beadle, J.J. Caudell, N. Chau, D. Deschler, et al., Management of salivary gland malignancy: ASCO guideline, J. Clin. Oncol. 39 (2021) 1909–1941.
[26] L.C. Silva, M.E. Pérez-de-Oliveira, C.M. Pedroso, A.A. Leite, A.R. Santos-Silva, M. A. Lopes, et al., Systemic therapies for salivary gland carcinomas: an overview of published clinical trials, Med. Oral Patol. Oral Cir. Bucal. (2024) e280–e287.
[27] M. Manou, D.S. Kanakoglou, T. Loupis, D.M. Vrachnos, S. Theocharis, A. G. Papavassiliou, et al., Role of histone deacetylases in the pathogenesis of salivary gland tumors and therapeutic targeting options, Int. J. Mol. Sci. 24 (2023) 10038.
[28] P.S.S. Pina, Y. Jang, C. Emerick, J.F. Scarini, S.C.O.M. Sousa, C.H. Squarize, et al., Novel epigenetic modifiers of histones presenting potent inhibitory effects on adenoid cystic carcinoma Stemness and invasive properties, Int. J. Mol. Sci. 25 (2024) 1646.
[29] L.O. Almeida, D.M. Guimarães, M.D. Martins, M.A.T. Martins, K.A. Warner, J. E. Nör, et al., Unlocking the chromatin of adenoid cystic carcinomas using HDAC inhibitors sensitize cancer stem cells to cisplatin and induces tumor senescence, Stem Cell Res. 21 (2017) 94–105.
[30] K.A. Warner, A.E. Oklejas, A.T. Pearson, Z. Zhang, W. Wu, V. Divi, et al., UM-HACC-2A: MYB-NFIB fusion-positive human adenoid cystic carcinoma cell line, Oral Oncol. [Internet]. 87 (2018) 21–28. Available from, https://linkinghub.elsevier.com/retrieve/pii/S1368837518303658.
[31] M.D. Martins, F.M. Silveira, M.A.T. Martins, L.O. Almeida, V.S. Bagnato, C. H. Squarize, et al., Photobiomodulation therapy drives massive epigenetic histone modifications, stem cells mobilization and accelerated epithelial healing, J. Biophotonics 14 (2021).
[32] A.F. McDonagh, Phototherapy: from ancient Egypt to the new millennium, J. Perinatol. 21 (2001) S7–12.
[33] Guimarães L. DA, L.P. Webber, E.J. Gaio, D.S. Junior, P. Gonçalves, M.J. Wick, et al., Using PDX animal models to identify and stratify adenoid cystic carcinoma patients presenting an enhanced response to HDAC inhibitors, Am. J. Cancer Res. 13 (2023) 143–160.
[34] A. Barasch, J. Raber-Durlacher, J.B. Epstein, J. Carroll, Effects of pre-radiation exposure to LLLT of normal and malignant cells, Support Care Cancer 24 (2016) 2497–2501.
[35] Y.-Y. Huang, S.K. Sharma, J. Carroll, M.R. Hamblin, Biphasic dose response in low level light therapy – an update, Dose-Response 9 (2011).
[36] S.-R. Tsai, M.R. Hamblin, Biological effects and medical applications of infrared radiation, J. Photochem. Photobiol. B 170 (2017) 197–207.
[37] V.H. Schartinger, O. Galvan, H. Riechelmann, J. Dudás, Differential responses of fibroblasts, non-neoplastic epithelial cells, and oral carcinoma cells to low-level laser therapy, Support Care Cancer 20 (2012) 523–529.
[38] M.D. Martins, F.M. Silveira, L.P. Webber, V.P. Wagner, M.A.T. Martins, C. H. Squarize, et al., The impact of photobiomodulation therapy on the biology and behavior of head and neck squamous cell carcinomas cell lines, J. Photochem. Photobiol. B 209 (2020).
[39] F.M. Silveira, T.R. Schmidt, B. Neumann, C. Rosset, V.G. Zanella, G.S. Maahs, et al., Impact of photobiomodulation in a patient-derived xenograft model of oral squamous cell carcinoma, Oral Dis. 29 (2023) 547–556.
[40] G.E. Djavid, B. Goliaie, A. Nikoofar, Analysis of Radiomodulatory effect of low-level laser irradiation by Clonogenic survival assay, Photomed. Laser Surg. 33 (2015) 452–459.